Indian Journal of Engineering & Materials Sciences
Vol. 30, February 2023, pp. 87-93
DOI: 10.56042/ijems.v1i1.60109

Influence of parameters on mechanical and micro-structural properties of tungsten inert gas (TIG) welded joint of 1 mm thin Inconel 625 plates

Saurabh Tripathi[a], Nehem Tudu[b], Mayuri Baruah[a, b*], Raj Ballav[b], & Shashi Bhushan Prasad[b]

[a]Department of Mechanical Engineering, Indian Institute of Technology Kharagpur, West Bengal 721302, India

[b]Production and Industrial Engineering Department, National Institute of Technology Jamshedpur, Jharkhand 831014, India

Received: 3 February 2022; Accepted: 28 November 2022

Inconel 625 (IN625), since its invention, has been a material of choice for industries where components in service conditions are exposed to extremely high temperatures, corrosion, and oxidation environments. As per the American welding society for butt-joining such alloys in sheets, non-traditional techniques are the best means for producing permanent joints. These techniques require high-cost setup and high maintenance costs which are only economical for high-volume assembly line fabrication in mass-production facilities. Therefore, Tungsten Inert Gas (TIG) welding is highly suitable for producing defect-free autogenous weldments in high-strength alloy sheets with a thickness below 3mm. The current work focuses on the experimental investigation of the TIG welding of Inconel 1mm sheets. In this work, mechanical properties and microstructure are studied for controlled heat input of TIG welding. Current is varied from 40A to 65A and voltage from 10V to 12V. Only three combinations of parameters show sound weld visually and are analyzed by performing various testing. The main objective of the study is to find the feasible process parameters for the micro joining of IN625 sheets. From this discussion, it appears that arc energy, welding current, and voltage significantly affect the quality of the weld.

Keywords: Tungsten inert gas (TIG) welding, Inconel 625 (IN625), Arc energy, Welding current, Voltage

1 Introduction

Inconel 625, a Ni–Cr–Mo–Nb solid–solution strengthened multi-component alloy with closed packed face centre cubic (fcc) austenitic matrix. It has been a material of choice for aeronautical, chemical, marine, and nuclear industries since its invention in 1962 at Inco Alloys International, Huntington.[1,2] The driving force behind such a wide range of applications is the appreciable combination of properties such as low and elevated temperature, yield tensile and creep strength (promoted by chromium, molybdenum, and niobium γ matrix stiffeners). It has good weldability and resistance to the oxidizing and corrosive environments (promoted by forming Cr_2O_3, Al_2O_3, and nickel oxide films over the external surface).[3–5]

This alloy was initially designed to be used in solid solution-strengthened conditions. However, it derives additional high-temperature strength and corrosion resistance when exposed to high service temperatures. This results in age–hardening derived from the precipitation of secondary phases, which includes intermetallic phases (promoted by the presence of Nb, Al, and Ti) such as γ′ and γ″. γ′—fcc ordered phases having Ni_3(Al, Ti) as elemental composition and γ″—body centre cubic (bcc) ordered phase having Ni_3 (Nb, Al, Ti) as elemental composition forming in the temperature range of 823 to 1023K.Intermetallic phases forms within the grain boundaries and precipitation of metal carbides (promoted by the presence of Fe and C as alloying elements) such as MC, $M_{23}C_6$, M_6C and M_7C_3 along the grain boundaries in the temperature range of 1033—1253 K.[6]

Though favorable for high-temperature applications, these strengthening phases reduce the ductility, toughness, and most importantly, the weldability of the alloy, thus impairing the high-temperature fabrication. The presence of these above-mentioned secondary phases results in the susceptibility of the alloy to hot cracking in heat affected zone (HAZ) during welding and post-weld heat treatment strain–age cracking in the heat affected and/or fusion zone (HAZ and/or FZ) in the presence of residual stresses induced due to fabrication or service conditions.[6]

Prasad et al. have performed the autogenous square butt joint welding of IN625 metal bellows of the wall thickness of 0.25 mm using pulsed micro plasma arc welding in the presence of argon shielding. Welding was done without edge preparations and determined the optimized values of peak current, base current,

*Corresponding author (E-mail: mayuri.prod@nitjsr.ac.in)

pulse width, and frequency using grey relational analysis.[7] Baruah et al. optimized the process parameter by trial-and-error method for pulsed micro plasma arc welding of 1 mm thickness IN625 plate in butt configuration to achieve sound weld.[8] Nagaraju *et al*. obtained optimum parameters for pulsed Nd: YAG laser beam welding of IN625 to achieve the best weld penetration and bead geometry using response surface methodology.[9]Ashtianiand Zarandooz have performed the resistance spot welding of IN625 0.7 mm sheets and used two-dimensional finite element methods to predict the electrode indentations and size of weld nuggets at different current intensities, weld cycles, and electrode tip diameters.[10] Chen et al. studied the fatigue performance experimentally and numerically of the transient liquid phase–brazed alloy 625 of 1.27 mm thick sheets. Sheets were brazed in the single and double-lap configuration using Planicro–36M^{TM} paste and observed the static mechanical strength of the joint was corresponding to the base metal.[11]

These non–conventional welding techniques have emerged in the recent decade for Ni-based super alloys fabrication. Have overcome the fabrication difficulties associated with these alloys by providing proper control over heat input. But still have seen limited industrial applications since product life–cycle cost reduction is the main concern for both manufacturer and operator. However, conventional welding techniques like gas tungsten arc welding (GTAW), plasma transferred arc welding, etc., being more flexible and cost–efficient techniques, are still widely exploited in industries for both manufacturing and repair purposes of these alloys.[12] Thus, it is suitable to explore modification in existing conventional techniques.

GTAW technique is one of the very popular and multi-objective techniques. Since this technique forms less spatter, has low distortion, better weld beads, and is a high-quality process.[13,14] Many researchers implemented the techniques for various studies, such as optimizing the process parameters to obtain better joints.[13] Few studied the mechanical and micro-structural properties of the weld joint[15], and some have studied the effect of heat input on the weld joint properties.[16] Rodríguez et al., observed that low heat input increases the weld strength. Reduction in heat input reduces the formation of carbides, which in returnprevents the precipitations.[16]

The present work studies microstructure and mechanical properties on weld joints of 1 mm thin IN625 sheets. GTAW technique was used in micro–mode, i.e., with controlled low heat input, and explores the feasible weld ability parameters. For this study, welding current and voltage are varied, all other parameters are kept constant, and the temperature was measured during the process with the help of a thermocouple. Distortion analysis, micro-hardness, micro-structural analysis, and tensile test are done on the welded sample. The main objective of the study is to find the feasible process parameters for micro-joining of 1mm thin IN625 sheets.

2 Materials and Methods

The welding process material has a dimension of 100×50×1 mm and with as a received nominal composition, as shown in Fig. 1(i). The microstructure of the base material is represented in Fig. 1(ii), which shows the presence of a fine austenitic structure. This is also the reason for the high ductility of the material. Since the thickness is very small, no special edge preparation and filler material was required for the welding process. The plates were welded as the experimental setup, as shown in Fig. 1(iii). A semi-automated set-up having provisions for adjusting the linear welding speed using an inline traveling as shown. A specially designed fixture employing the copper back plate was used to avoid bending and distortions while welding.

The process parameters employed in the TIG welding of Inconel 625 were based on a trial-and-error approach. The speed was kept constant at 4.2 mm/s, and the current is varied from the lowest level possible. Welding is performed at various combinations, as shown in Table 1. It is found that after 65 A, the sheets were burnt through. Thus, three combinations of parameters are considered for analysis which shows proper welding. The weld beads obtained for sound welds as per visual inspection are shown in figure 1(iv).Arc energy is calculated using equation 1 to make a comparative study.

$$AE = \frac{60 \times V \times I}{1000 \times v} \quad \ldots(1)$$

Where AE is arc energy, V is voltage, I is welding current, and v is welding speed.

3 Results and Discussion

Inconel 625 (IN625) plates are joined in butt configuration as per the combination of parameters shown in Table 1. Different effects or quality of welding are observed at different combinations, which are presented in Table 1. Amongst all the

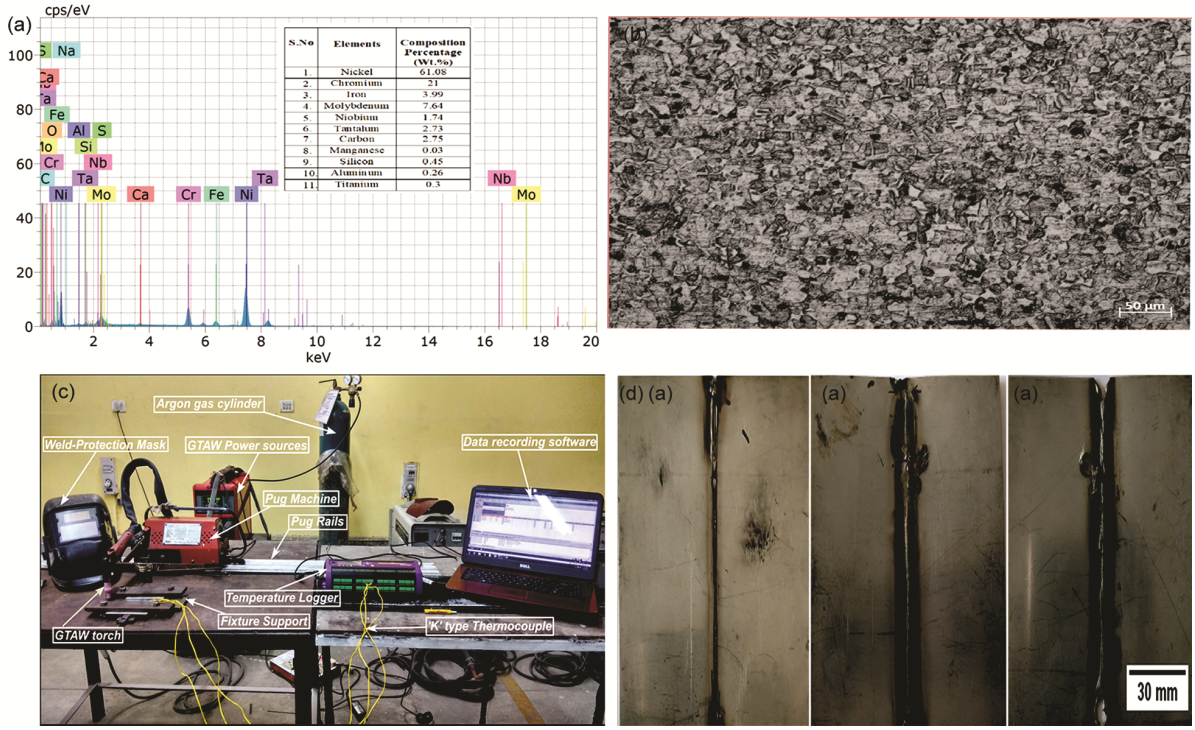

Fig. 1 — (i) EDX data showing composition of Inconel 625, (ii) microstructure of base metal, (iii) experimental setup, and (iv) welded sheets with current input (a) 50A, (b) 55A, and (c) 60A.

Table 1 — Process parameters for the experimentation

Exp. No	Current (A)	Voltage (V)	Speed (mm/s)	Arc Energy (kJ/mm)	Arc Length (mm)	Gas flow rate (L/min)	Gauge pressure (bar)	Quality or Effect
1	40	10	4.2	5.71	2	9	125	Only Heating*
2	50	10	4.2	7.14	2	9	125	Half Penetration
3	55	10	4.2	7.86	2	9	125	Welding (S1)
4	55	12	4.2	9.43	2	9	125	Welding (S2)
5	60	10	4.2	8.57	2	9	125	Welding (S3)
6	65	10	4.2	9.29	2	9	125	Burnt Through

combinations, only three combinations can create the sound weld. A sample of these weld joints is tested to study the effect and discussed.

3.1 Temperature measurement

The final weldment's quality greatly depends on the welding process, the peak temperature reached the thermal histories, and cooling rates. To measure the temperature during welding, K-type thermocouples are fixed at three locations on the plates' upper surfaces as shown in Fig. 2(i) (a). Point A and Point B are located at 3 mm from the weld centerline, and point C is located at 9 mm from the weld centerline. Time-temperature history at the three points is shown in Fig. 2(i) (b) for welding conditions of 60 A, 10 V, and 4.2 mm/s. It is seen that the peak temperature decreases as we move away from the weld centerline.

Time-temperature history for three different welding currents measured at 3 mm from the weld centerline is plotted in Fig. 2(ii) (a). It can be seen in Fig. 2(ii) (b) that the peak temperature increases with an increase in welding current. The heating rate is almost similar, whereas there is a variation in the cooling rate. The cooling rate, peak temperature, and temperature histories are responsible for the formation of the joints microstructure, which influence joint mechanical properties. The ratio of change in temperature with the change of time estimates the cooling rate. Figure. 2(ii) (c) depicts the cooling rate for three different welding conditions. It is seen that the cooling rate decreases with an increase in welding current. The microstructure formed after the welding process depends on the cooling rate. This explains the formation of different microstructures at three different zones.

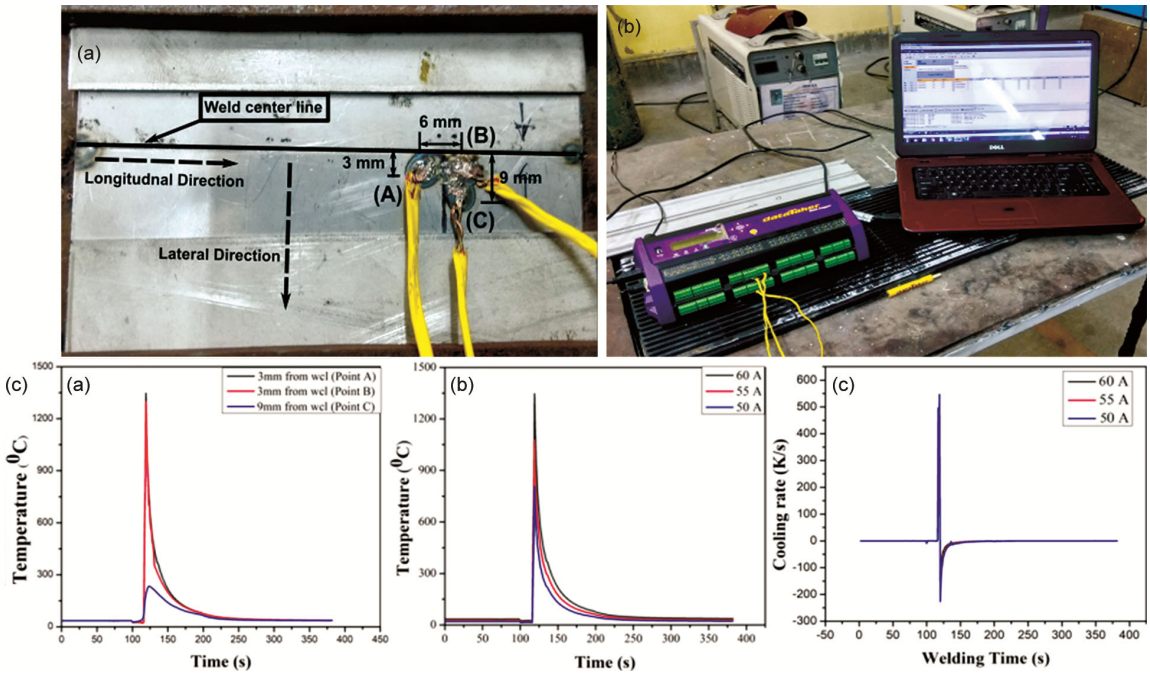

Fig. 2 — (i) Thermocouple connections with (a) the base plate, (b) data-logger and computer interface, and (ii) (a) Time-temperature curves for sample S2 at different locations (b) Time-temperature curves for samples S3, S2, and S1 (c) Cooling rates for samples S3, S2, and S1.

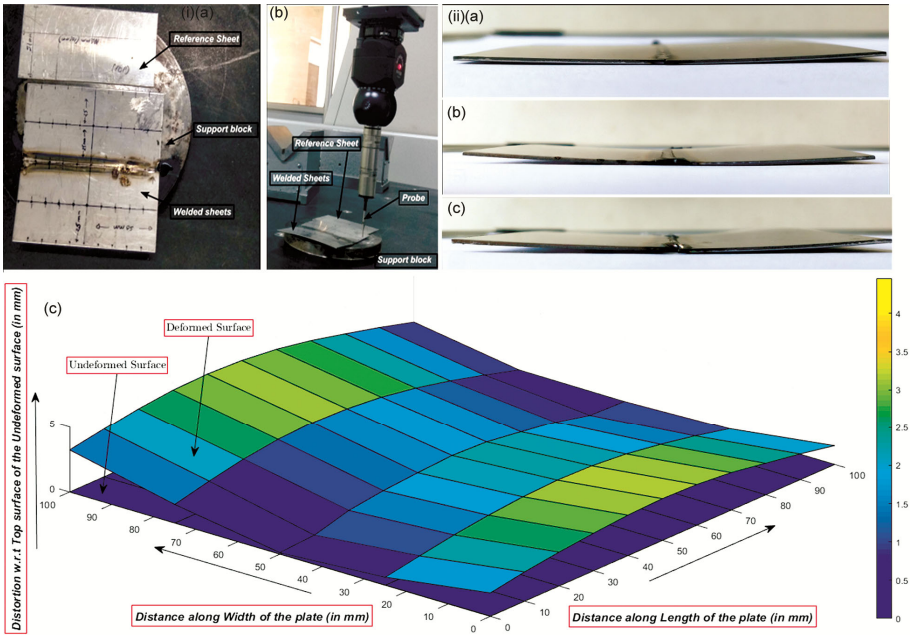

Fig. 3 — (i) Coordinate measuring machine, (ii) distortion in sheets with arc energy (A_E) (a) 7.86 kJ/mm, (b) 9.43 kJ/mm, and (c) 8.57 kJ/mm (iii) virtual visualization of distortion.

3.2 Distortion analysis

During the welding process, longitudinal and lateral distortion of the welded sheets occurs due to thermal stresses and strains generated during the process of rapid melting and solidifying of the base metal in joint area. A similar distortion can be seen in Fig. 3(ii) for samples S1, S2 and S3 welded respectively at 7.86, 9.43, and 8.57 kJ/mm arc energy (A_E). Further, from this figure, it can be concluded that as the heat input to the base metal increases during the welding process,, distortion also increases simultaneously.

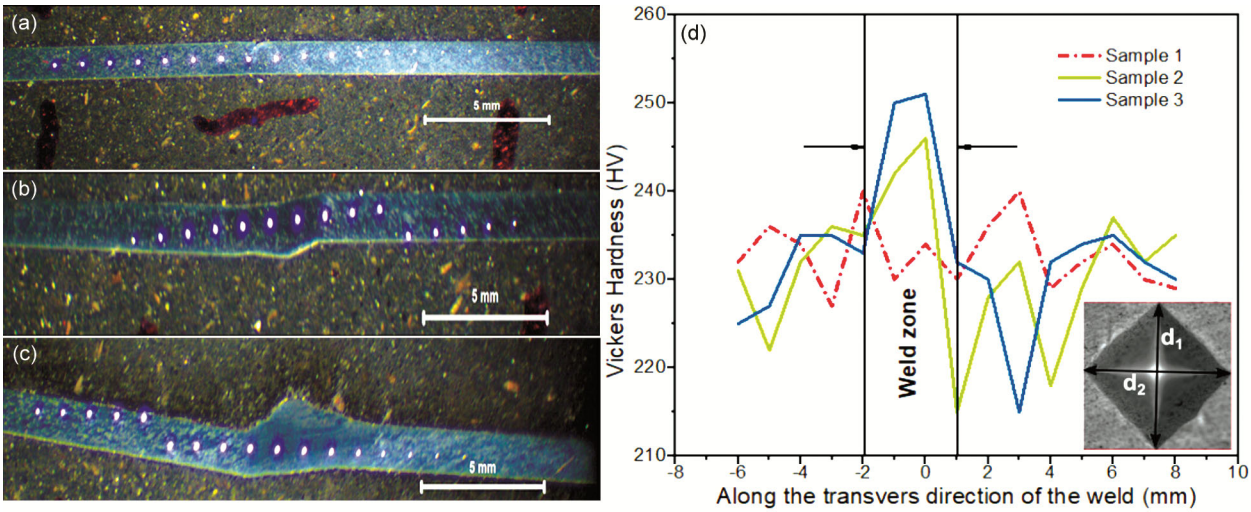

Fig. 4 — Traverse path of the micro-indentation of the sample (a) S1, (b) S2, (c) S3, and (d) graph of Vickers hardness data of the sample.

So, an attempt was made to experimentally measure this distortion by measuring the relative displacement of the top surface of the distorted sheet with respect to an un-distorted sheet's top surface in the Coordinate Measuring machine, as shown in Fig. 3(i). For this, welded sheets and an undistorted sheet were firmly attached to a base plate to keep its weld center line of the welded sample, as well as the undistorted sheet leveled along the horizontal surface, as shown in Fig. 3(i) (a). Taking this zero as the reference height along the Z-direction of the machine, the displacement of the various points marked on the surface of welded sheet was measured by bringing them in contact with the probe end of the machine.

The displacements thus obtained in the Z-direction for different points marked over the top surface of the distorted weldment (welded at parameter I = 55 A) were then plotted in MATLAB 2017, and a virtual visualization of the distortion is obtained, as shown in figure. 3(iii).

3.3 Hardness Testing

For hardness testing, each sample with phenolic resin mold around them was mounted on the vice of the Vickers micro-indentation machine, one at a time, and indentations were made in the transverse direction of the weld as shown in Fig. 4(a-c) with a gap of 1mm between two successive indentations. And the indentation load was kept at 500 kg-f with 10 s dwell time for each indentation. The result thus obtained was plotted as shown in Fig. 4(d), considering the centre in the transverse direction of the weld as reference or zero position. As per this figure, the micro-hardness values in the weldzone of S2 and S3 samples welded at 55 A and 60 A current and 12 V and 10 V voltage, respectively, are higher compared to other portions of the weld zone, which might be due to the formation of martensitic with fine columnar-dendritic structure and formation of laves phases. The micro-hardness in the case of the 55 A and 10 V weld is less, which could be due to the partial weld formation and misalignment between plated in the weldzone. From Fig. 4(d), it can be concluded that the higher the welding current and voltage, the higher the hardness of the weld zone.

3.4 Tensile testing

For tensile testing, three sub-size specimens as per the standard size were cut out from each of the welded samples. Then it was tested on the universal tensile testing machine 'Tinius Olsen H50KS', having a maximum capacity of 48 kN. The test was performed with a strain rate of 0.48 mm/min as per the standard ASTM E8/E8M.[17] Thus, stress-strain results were plotted separately as in Fig. 5(a). From this figure, it can be observed that the samples S1, S2,and S3 have yield strengths of 384, 742, and 564 MPa, respectively; ultimate tensile strengths of 384, 753, and 651 MPa, respectively, and total percentage elongation of 3.1, 30.3 and 18.06 % respectively. Further, the joint efficiencies are calculated using equation 2.

$$E_J = \frac{S_{UJ}}{S_{UP}} \times 100 \qquad \ldots(2)$$

S_{UJ} is the ultimate tensile strength of the joint, and S_{UP} is the ultimate tensile strength of the parent metal. And joint efficiencies calculated for

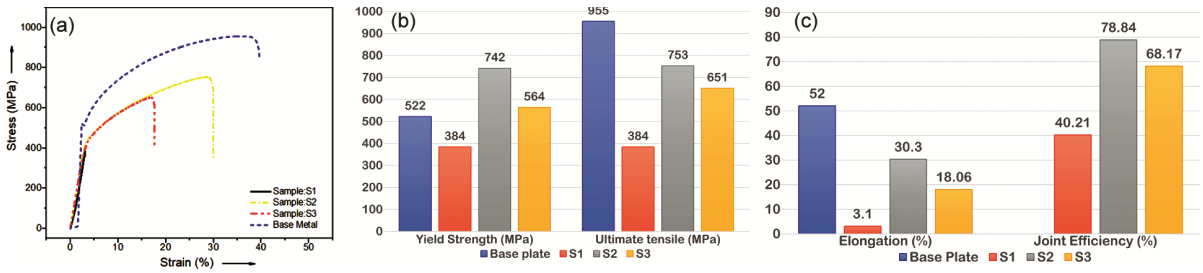

Fig. 5 — (a) Graph plot of tensile test, (b) comparison of yield strength and tensile strength, and (c) comparison of total elongation and joint efficiency.

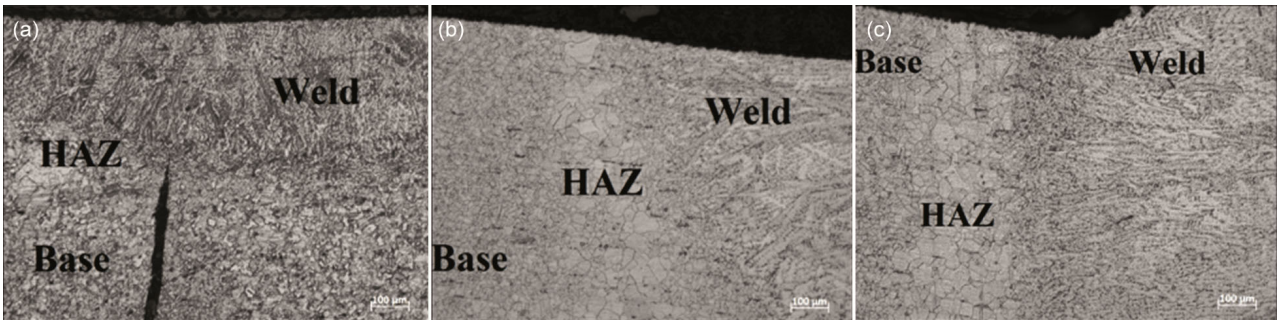

Fig. 6 — Micrographs of (a) S1, (b) S2, and (c) S3.

samples S1, S2, and S3 are 40.21, 78.84, and 68.17 %, respectively.

The yield strength and ultimate tensile strength of the joint are compared with the parent metal and shown in Fig 5(b). from this comparison, it is observed that in S2 and S3 sample yield strength of the welded sample is higher than the base metal. Amongst these, S2 shows the highest value of 742 MPa, i.e., at the parameter of 55 A current and 12 V voltage. Here, it can be concluded that yield strength, ultimate tensile strength, joint efficiency, and ductility are directly proportional to welding current, voltage, and arc energy.

3.5 Microstructure

The microstructure of the base material consisted of refine dequiaxed austenitic grains. A number of primary carbides and carbonitrides were also observed in the base material. The mean grain size number is 8.66 according to the ASTM E 1382. These alloys have good room-temperature ductility based on their austenitic (fcc) structure. The shape of the fusion zone obtained at 7.86 kJ/mm is regular and symmetric clearly defined by a semi-circular cross-sectional boundary as shown in Fig. 6(a). It is seen that in the case of low arc energy, misalignment of the sample takes place. Thus, very optimum arc energy is an utmost necessity of the process. It is found that the fusion zone size increases with an increase in arc energy. It is also reflected that the full penetration fusion zone is obtained at 8.57 kJ/mm and 9.43 kJ/mm as shown in Fig. (b) and (c). It is also found that no unacceptable porosity and cracks are observed in the fusion (FZ) or heat-affected (HAZ) zone at any welds.

The weld fusion zone exhibited a columnar dendritic structure in all three welding conditions. The columnar dendrite structure was mainly observed at a moderate cooling rate. It is well known that the scale of the dendritic structure is inversely proportional to the cooling rates. Thus, the rapid weld metal cooling rate at a lower welding current resulted in the formation of a very fine dendritic structure in the weld fusion zone compared to a higher welding current. The dendrites in the weld fusion zone are very fine and equiaxed in the weld interior and are slightly coarser and columnar at regions adjacent to the fusion boundary.

In the case of low arc energy (7.86 kJ/mm), HAZ was observed to be extremely narrow with no significant grain growth. When the weld heat input is low, and temperature gradients in the HAZ are steep, little grain growth in the HAZ is expected. While in the case of weld joints with 8.57 kJ/mm and 9.43 kJ/mm, significant grain growth in the HAZ zone is seen. The average grain size number is 5.33 and 6.17 in the case of 8.57 kJ/mm and 9.43 kJ/mm, respectively. Thus, the grains become coarser with increasing arc energy.

4 Conclusion

With the ever-increasing demand for the microscale manufacturing process, different fabrication techniques are being developed and analyzed. Microwelding is a developed joining processes where the intense and regulated heat source is useful to fuse the material over a narrow zone. Therefore, the evolution of the parametric domain for -free weld joints is a significant contribution to the present research work. TIG welding for joining 1 mm thin sheets of Inconel 625 is investigated in the present work. From this study, it can be concluded that peak temperature is directly proportional to welding current. In contrast, the heating rate is not affected, but the cooling rate does and is inversely proportional to the welding current. Distortion, yield strength, ultimate tensile strength, ductility, joint efficiency, fusion zone size, and grain size increase with increased welding current, voltage, and arc energy. Whereas heat affected zone is steeper when there is an increase in arc energy. At low arc energy and welding current, the sample's misalignment may occur, and fine dendritic structure in the weld fusion zone occurs. The weld zone's hardness is directly proportional to the welding current and voltage. Thus, this discussion shows that arc energy, welding current, and voltage significantly affect the weld quality. The higher the arc energy, welding current, and voltage, the better the weld quality. Therefore, from the selected process parameters, the parameter for S2 (I = 55 A, V = 12 V and A_E = 9.43 kJ/mm) is the optimum parameter. Thus, proper optimization of process parameters can be performed by considering more range of input parameters.

5 Acknowledgements

The author acknowledges Dr. Arpan Kumar Mondal, Assistant professor, National Institute of technical teachers training and research, Kolkata, to provide the experimental setup. Also, to the National Institute of Technology Jamshedpur for funding as a fellowship and to the Indian Institute of Technology Kharagpur and Adityapur Autocluster to conduct testing.

References

1 Oliveira M de, Couto A, Almeida G, Reis D, Lima N de & Baldan R, *Metals (Basel),* 9 (2019) 301; doi: 10.3390/met9030301.

2 Tudu N, Baruah M, Prasad S B & Paul C P, in *Next Generation Materials and Processing Technologies: Select Proceedings of RDMPMC 2020,* edited by Bag S, Paul C P & Baruah M(Springer Nature, Singapore), 2021, 185; doi: 10.1007/978-981-16-0182-8_15.

3 Ruiz-Vela J I, Montes-Rodríguez J J, Rodríguez-Morales E & Toscano-Giles J A,*Weld World,* 63 (2019)459; doi: 10.1007/s40194-018-0661-z.

4 Tudu N, Baruah M & Prasad S B, *Sci Technol Weld Join,*(in press); doi: 10.1080/13621718.2022.2156715.

5 Tudu N, Baruah M & Prasad S B, *Rapid Prototyp J,*(in press); doi: 10.1108/RPJ-08-2021-0219.

6 Volpato G M, TetzlaffU & Fredel M C *Addit Manuf,* 55 (2022) 102871; doi: 10.1016/j.addma.2022.102871.

7 Prasad K S, Chalamalasetti S R & Damera N R, *Int J Adv Manuf Technol*, 78 (2015) 625; doi: 10.1007/s00170-014-6665-y.

8 Baruah M, Prasad S B, Tudu N, Murmu B K & Singh S, *Mater Today Proc,* 33 (2020) 5751 doi: 10.1016/j.matpr.2020.06.604.

9 Nagaraju U, Gowd G H & Vardan T V, *Mater Today Proc*, 5 (2018) 7991; doi: 10.1016/j.matpr.2017.11.483.

10 Ashtiani H R R & Zarandooz R, *Metall Mater Trans A Phys Metall Mater Sci*, 46 (2015) 4095; doi: 10.1007/s11661-015-3030-1.

11 Chen J, Demers V, Turner D P & Bocher P *Metall Mater Trans A Phys Metall Mater Sci*, 49 (2018) 1244; doi: 10.1007/s11661-018-4474-x.

12 Stewart M. *Fabrication, Welding, and in-Shop Inspection*. In: Surface Production Operations Elsevier; 2021; p. 197; doi: 10.1016/B978-0-12-803722-5.00006-9.

13 Choudhury B, Chandrasekaran M, Tamang S & Teyi N *Optimization Study on GTAW of Inconel 825 Using Desirability Function Analysis (DFA)*, paper presented at 6th International & 27th All India Manufacturing Technology, Design and Research Conference (AIMTDR-2016) 2016.

14 Kanemaru S, Sasaki T, Sato T, Mishima H, Tashiro S & Tanak M, *Weld World* 58 (2014) 11; doi: 10.1007/s40194-013-0090-y.

15 Cortés R, Barragán E R, López VH, Ambiz R R & Jaramillo D, *Int J Adv Manuf Technol,* 94 (2018) 3949–3961; doi: 10.1007/s00170-017-1128-x.

16 Rodríguez NK, Barragán ER, Lijanova I V., Ambriz R R & Jaramilo D, in*Proceedings of the 17th International Conference on New Trends in Fatigue and Fracture*,edited byedited by Ambriz R, Jaramillo D, Plascencia G & Abdelaziz M N (Springer International Publishing: Cham, Switzerland), 2018, 255; doi: 10.1007/978-3-319-70365-7_29.

17 Lader S K, Baruah M and Ballav R, *J Manuf Process,* 85 (2023) 1154; doi: 10.1016/j.jmapro.2022.12.033.